Nanofracture in graphene under complex mechanical stresses

Bin Zhang, Lanjv Mei, and Haifeng Xiao

Citation: Appl. Phys. Lett. **101**, 121915 (2012); doi: 10.1063/1.4754115
View online: http://dx.doi.org/10.1063/1.4754115
View Table of Contents: http://apl.aip.org/resource/1/APPLAB/v101/i12
Published by the American Institute of Physics.

Nanofracture in graphene under complex mechanical stresses

Bin Zhang,[a] Lanjv Mei, and Haifeng Xiao
State Key Laboratory of Mechanics and Control of Mechanical Structures and College of Aerospace Engineering, Nanjing University of Aeronautics and Astronautics, Nanjing 210016, China

(Received 2 July 2012; accepted 4 September 2012; published online 20 September 2012)

Nanoscale fracture of graphene under coupled in-plane opening and shear mechanical loading is investigated by extensive molecular dynamics simulations. Under opening-dominant loading, zigzag edge cracks grow self-similarly. Otherwise, complex stresses concentrated around crack-tip can manipulate the direction of crack initiation changing by 30° (or multiples of 30°). Toughness determined by obtained critical stress intensity factors 2.63–3.38 nN $Å^{-3/2}$ demonstrates that graphene is intrinsically brittle opposite to its exceptional high strength at room temperature. Torn zigzag edges are more energetically and kinetically favorable. Cracking of graphene has dependences on local stresses, edge energy, and dynamic effects, which provides a possible way to regulate graphene edges. © *2012 American Institute of Physics*. [http://dx.doi.org/10.1063/1.4754115]

Graphene, as an atom-thick carbon sheet, is extensively studied for the successful laboratory exfoliation,[1,2] and it has attracted tremendous attention from the scientific community for its remarkable mechanical and electrical properties that are currently being explored for a number of applications including nanoelectromechanical systems, nano-electronics, etc. Recent mechanical experiments have shown that graphene is the strongest material measured hitherto with an elastic modulus of 1.0 TPa,[3] which exceeds those of any previously existing materials. Rafiee *et al.*[4] also reported that graphene as reinforcement has extraordinary effectiveness to resist fracture and fatigue in composites. However, Hashimoto *et al.*[5] provided a direct experimental evidence for the existence of defects in graphene layers. The extraordinary mechanical properties can be affected by the presence of defects that cause a more reduction of the strength. The existing works have treated defects in graphene as cracks that can initiate fracture.

The research on fracture of graphene can date back to the simulations conducted by Omeltchenko *et al.*[6] in which a notched graphite sheet was loaded uniaxial tension and then underwent cleavage. However, that retention of the cutoff function of early version potential makes the quantitative aspects of results questionable. Recently, Belytschko *et al.*[7–9] carried out series of theoretical researches on the fracture of pre-cracked graphene under uniaxial tensile loading. The critical stress intensity factors under pure opening loading were obtained for zigzag and armchair cracks, while the propagation direction was manually specified. Lu *et al.*[10] also investigated fracture of graphene nano-ribbons (GNRs) under uniaxial tension. Furthermore, shear deformation plays an important role in the wrinkling and rippling behavior of graphene, which, in turn, controls charge carrier scattering and electron mobility.[11] It is even possible to modulate the graphene energy-gap from 0.0 to 0.9 eV by combining shear deformations with uniaxial strains.[12] In point of fact, mixed-mode fracture inevitably occurred during the tearing of graphene sheets from graphite or other substrates to obtain free-standing sheets or narrow ribbons.[13] In Ref. 6, multiple cracks branched sprouting off the primary crack front, thus tilted cracks were basically under mixed tensile and shear loading. Besides theoretical studies, Kim *et al.*[14] presented explorations on tearing suspended monolayer graphene membranes by high-resolution transmission electron microscopy (HRTEM). However, radiation damage by electron-beam energy and applied dose cannot be neglected for light element materials due to the limitations of HRTEM.[15] It is still a challenge to observe experimentally the cracking of graphene under pure mechanical loading without electromechanical coupling effects.

Thus far, complex mechanical loading is rarely considered in previous works on fracture in graphene. Herein we will show our extensive molecular dynamics (MD) simulations on nanoscale fracture of graphene under coupled opening and in-plane shear loading of far-field (I/II mixed-mode fracture). The modified second-generation reactive empirical bond-order (REBO) potential[16] is used by shifting the cut-off distance and removing cut-off function to avoid unphysical dramatic increase in the interatomic force. The evolution of atomically cleaving of graphene is then revealed without manually specified direction of crack propagation.

The well established REBO potential has been widely used[6,10,17–19] to specifically describe the interatomic interaction of carbon atoms; two cutoff distances 1.7 Å and 2.0 Å are initially set for a smooth transition of cutoff function from 1 to 0 to limit the range of covalent interactions as the interatomic distance increases. However, such a cutoff function generates spurious bond forces near the cutoff distance, which will lead to unphysical results due to discontinuity in the second derivative of the cutoff function.[20,21] In this study, the cutoff function is taken to be 1.0 within a cutoff distance of 1.92 Å (Ref. 22) and zero otherwise to avoid such artifact defect.

A size-reduced model containing a small circular-shaped domain cut from the crack tip is utilized to model semi-infinite cracks in real graphene. A reasonable domain size is chosen so that its outer boundary falls in the *K*-dominant zone, which can make all-atom simulations

[a]Author to whom correspondence should be addressed. Electronic mail: beenchang@nuaa.edu.cn.

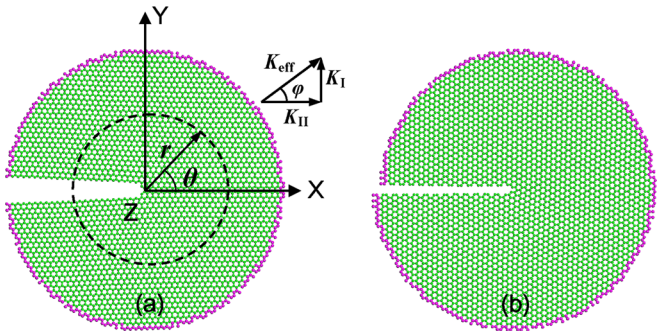

FIG. 1. Boundary layer MD models and coordinates. A pre-existing straight crack along (a) zigzag or (b) armchair edge is embedded in a two-dimensional graphene lattice (green). The outer boundary layer (pink atoms) is subject to displacement loadings, (a) opening and/or (b) in-plane shear. Origins are at the concave crack tips located either at (a) a bond or (b) an atom.

computationally efficient. Afterwards, we consider an initially straight crack subject to in-plane opening and shear loading characterized by the local stress intensity factor (SIF) K field. Two prevalent cracks with orientations along ZZ or AC edges are shown in Figure 1. Two or three rows of atoms are removed to generate cracks in our models, and the distance between two crack surfaces is big enough to avoid self sealing, especially in pure shear case. The length of crack is more than 10 times lattice spacing to avoid unphysical Griffith fracture stress and flaw insensitiveness.[23] A total of around 4000 carbon atoms in our disk model with a radius $r = 60$ Å are initially relaxed until the energy of the system is fully minimized at a specified temperature. The thickness of graphene is assumed to be 3.335 Å under plane stress condition. Hereafter our results are divided by 3.335 Å to make connection of a two-dimensional lattice with a three-dimensional solid.

Williams[24] has given the asymptotic expansion of the displacement field around the crack tip in an isotropic linear elastic body. At a given SIF K^{app} applied by far-field loadings, the crack-tip asymptotic solution is as[25]

$$u_x = \frac{1+v}{E}\sqrt{\frac{r}{2\pi}}\left[K_I^{app}\cos\frac{\theta}{2}\left(k-1+2\sin^2\frac{\theta}{2}\right) + K_{II}^{app}\sin\frac{\theta}{2}\left(k+1+2\cos^2\frac{\theta}{2}\right)\right], \quad (1)$$

$$u_y = \frac{1+v}{E}\sqrt{\frac{r}{2\pi}}\left[K_I^{app}\sin\frac{\theta}{2}\left(k+1-2\cos^2\frac{\theta}{2}\right) - K_{II}^{app}\cos\frac{\theta}{2}\left(k-1-2\sin^2\frac{\theta}{2}\right)\right], \quad (2)$$

where radius r and polar angle θ are depicted in Figure 1(a), u_x and u_y are displacements in X and Y directions, respectively. Young's modulus E is 1.0 TPa,[3] Poisson's ratio v is 0.165,[26] and $k = (3-v)/(1+v)$ for plane stress here. K_I^{app} and K_{II}^{app} are SIF components specified by opening and shear stresses. Phase angle φ (loading mixed parameter or equivalent crack angle) is defined as $\varphi = \tan^{-1}(K_I^{app}/K_{II}^{app})$, and an effective SIF K_{eff}^{app} at the initial crack length is evaluated as $K_{eff}^{app} = \sqrt{(K_I^{app})^2 + (K_{II}^{app})^2}$, see Figure 1(a). Therefore the far-field behavior of pristine graphene is assumed to be well-represented by the solution since the stress singularity decreases apart from the crack tip. The boundary condition is similar to a suspended graphene spanning a hole in the TEM grid.

Mixed-mode loading in classical fracture mechanics is then imposed by initially assigning all atoms in the displacement field given by the crack-tip asymptotic solution of a specified initial K_{eff}^{app}. In Figure 1, atoms (pink) on the outer boundary layer are held fixed, while all the other atoms (green) are set free. Moreover, we implement the deformation-control method by applying displacement increments gradually to the fixed boundary layer (pink) separately every 500 MD steps. At each applied loading, the statically equilibrium lattice structure is calculated to minimize the total energy by the limited memory BFGS geometry optimization algorithm;[27] thereby, local energy minimum configurations are obtained. The velocity-Verlet time stepping scheme is used with a time step 1.0 fs at 300 K predominantly with a Berendsen thermostat, and this yields a maximal strain rate ~ 0.0002 ps^{-1} primarily. We note that MD simulations are often sensitive to the temperature control and the loading rate; thus, our results mainly provide a qualitative understanding of the fracture mechanisms.

The energy-balance criterion by Griffith is the fundamental fracture criterion for brittle continua, which states that a crack meets the critical growth condition when the net change in the total energy of the system vanishes upon crack extension by an infinitesimal distance.[28] Using the relationship between the critical SIF of Griffith K_{th}^c and the energy release rate (twice of the surface energy density γ_s) for linear elastic materials, one has $K_{th}^c = \sqrt{2E\gamma_s}$.[25] Since E is assumed isotropic for graphene, K_{th}^c will be mainly determined by γ_s. By use of $\gamma_s = 1.041$ eV/Å and 1.091 eV/Å (Refs. 29 and 30) for ZZ and AC cracks, we get $K_{th}^c = 3.162$ nN Å$^{-3/2}$ and 3.238 nN Å$^{-3/2}$, respectively.

TABLE I. Critical effective stress intensity factors K_{eff}^c (nN Å$^{-3/2}$) of ZZ and AC cracks in graphene under mixed-mode far-field loading at various phase angles φ.

φ		0°	15°	30°	45°	60°	75°	90°	90°	90°	90°	90°	90°
K_{eff}^c	ZZ	3.06	2.75	2.63	2.90	3.15	3.02	3.05	3.16[a]	4.21[b]	2.64[c]	6.0[d]	10.32[e]
	AC	2.87	3.30	3.28	2.87	2.78	2.85	3.38	3.24[a]	3.71[b]			

[a] K_{th}^c.
[b] Reference 7.
[c] Reference 8.
[d] Reference 6.
[e] Reference 31.

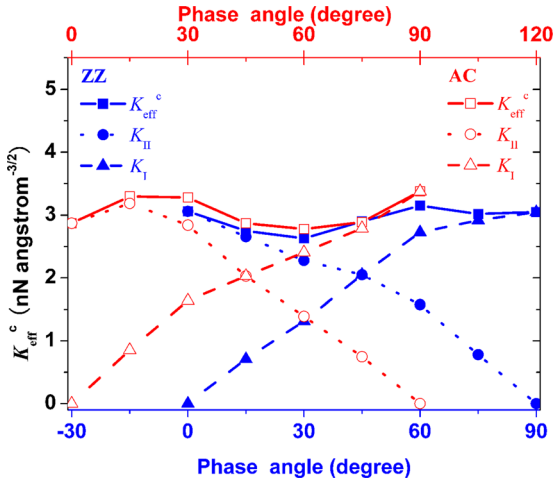

FIG. 2. Critical effective stress intensity factors K_{eff}^c of graphene cracks (ZZ in blue and AC in red) varying with phase angles φ of far-field loading. K_{I} and K_{II} are opening and shear components of K_{eff}^c.

In Table I and Figure 2, our results show that the critical effective SIF K_{eff}^c of I/II mixed-mode loading falls in the range between 2.63 nN Å$^{-3/2}$ and 3.38 nN Å$^{-3/2}$ varying with φ, relatively low compared to steel, which reveals that graphene is brittle at 300 K opposing its ultrahigh strength. As the difference of geometric chiral angle between AC and ZZ edges is 30°, similar trends for K_{eff}^c are perceived if φ is shifted by 30°. K_{eff}^c of ZZ cracks are slightly lower indicating smaller toughness; thus, graphene is easier to break along ZZ direction. For ZZ cracks under pure opening tension ($\varphi = 90°$), our K_{eff}^c are reasonable with theoretical K_{th}^c, and compared with available reported datum, see Table I, the discrepancy may be due to different crack models[6,8] and potentials used therein.[7,31]

With an available small increasement of loading $\Delta K_{\text{eff}} \approx 0.01$ nN Å$^{-3/2}$ within 500 fs, the first bond is broke abruptly between two orange atoms that are most stretched, subsequently accompanied with disruption of adjacent bonds exhibiting a dynamic fracture process, see Figure 3. Compared with the original configurations in Figure 1, the various sites of bond breaking are not certainly at the original tips. Asymmetric cleavage (only symmetric cleavage in Figure 3(f) for a ZZ crack under pure tension) demonstrates that brittle fracture via bond breaking prevails at room temperature. This causes a shift of the fracture path downward relative to the primary crack. The carbon atoms bounce off each other after bond breaking, which accelerates crack extension and significantly relaxes local stress at the crack-tip, see also Figure 5, leading to evident internal displacements in Figures 3(c), 3(g)–3(i). The energy flow of external work into graphene increases the crack-tip speed, where local cracks sprout to facilitate the dissipation of energy. In Figure 3(c), the crack-tip speed can even reach ~2.0 km/s around 16% of the calculated Rayleigh wave speed for the graphite sheet (12.4 km/s)[6] under current loading strain rates.

Up to now, no single criterion in classical continuum mechanics can give satisfactory predictions for crack initiation direction under complicated loading conditions. All existing criteria predict that a crack under mode II (in-pane shear, $\varphi = 0°$) loading propagates along about a 70° direction with respect to the original crack line. However, a mode II crack either propagates in mode I (opening, $\varphi = 90°$) or mode II, depending on material properties and load magnitudes.[32] Continuum criteria seem to lose efficacy in predicting direction of crack initiation in graphene. In Figures 4(a)–4(d), new cracks in ZZ crack models initiate in the direction of an angle $\beta = 120°$ deviating from the original edge when in-plane shear loading is prevailing, β maintains unchanged till $\varphi = 60°$, and fresh edges are in zigzag (blue). Further increasing φ will induce the transition of β. At $\varphi = 65°$, β changes to 150° and fresh edges are in armchair (red), see Figure 4(e). This configuration coincides with the prediction that zigzag-armchair junctions with an angle of 150° would be more stable.[6,33] Once $\varphi > 65°$, opening loading becomes dominant, crack grows self-similarly along original direction, and fresh edges are in zigzag again, see Figure 4(f).

For AC crack models, initiation angle $\beta = 90°$ at $\varphi = 0°$ in Figure 4(g), new crack-tip nucleates prior to primary tip, and fresh edges are in zigzag. At $\varphi = 26.5°$ in Figure 4(h), propagating direction changes to 120°, and fresh edges are in armchair. When $\varphi > 26.5°$ in Figures 4(i)–4(l), β transforms to 150° and keeps unchanged till $\varphi = 90°$, and fresh edges are in zigzag again.

Fresh edges exhibit mostly in zigzag, and armchair edges can be formed under particular stress conditions

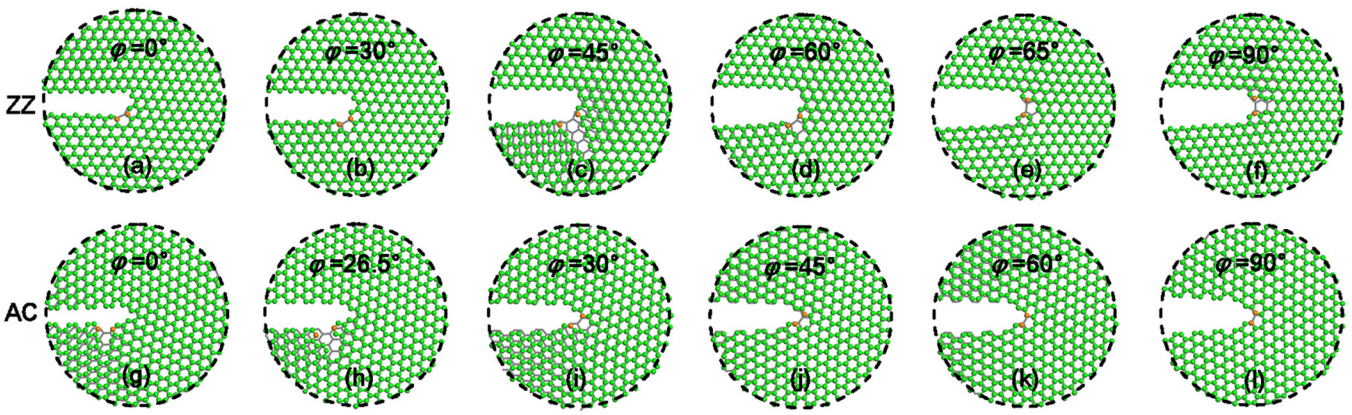

FIG. 3. Snapshots ($r = 20$ Å insets from the whole model in Figure 1) of crack initiations in graphene lattices (green) under critical loads K_{eff}^c, overlapped with previous configurations (grey lattices) to depict the local bond breaking. (a)–(f) ZZ crack models at $\varphi = 0°$, 30°, 45°, 60°, 65°, and 90°; (g)–(l) AC crack models at $\varphi = 0°$, 26.5°, 30°, 45°, 60°, and 90°, respectively. The atoms where the first bond is broke are marked in orange.

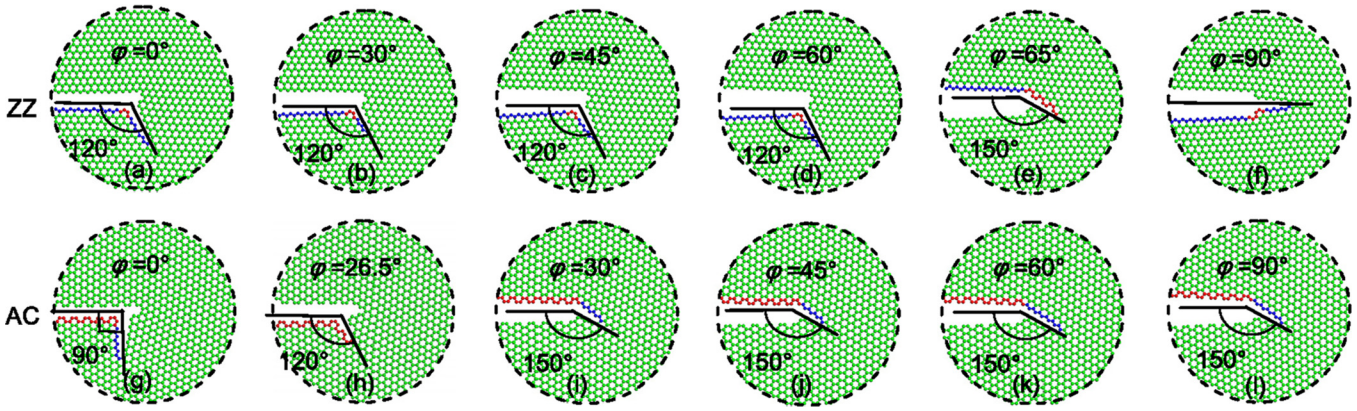

FIG. 4. Snapshots ($r = 30$ Å) of crack propagation after initiation in Figure 3 under complex mechanical stress. The angle of crack propagation β orienting to primary crack is depicted correspondingly. ZZ crack edges are rendered in blue, AC in red.

during the transition of propagating direction. Under loading $K_{\text{eff}}^{app} = 3.21$ nN Å$^{-3/2}$ at $\varphi = 65°$ in Figure 4(e), zigzag crack kinks and armchair edge is formed. In Figure 4(h), armchair crack turns its direction with 120° followed by armchair edge under $K_{\text{eff}}^{app} = 3.25$ nN Å$^{-3/2}$ at $\varphi = 26.5°$. This is similar to experimental tears kinking within graphene membrane under only complex mechanical stress applied by circular boundary of the Quantifoil holey carbon TEM grid.[14]

With the increasing of complex loading, stresses concentrated around crack tip morph the hexagonal carbon rings into deformed shapes, see also supporting movies in Figure 5. Once the bonds are rotated or broken, the hexagonal symmetry of the graphene lattice is destroyed, which leads to crack kinking, and AC edges subsequently are formed at turns. The dynamic effect of fast fracture in MD simulations can also cause kinking, while branching is not observed. Bond rotation by 90° with the formation of 5-7 SW defects (black rings) can be noticed around the primary tips in Figures 5(a) and 5(g) and at the turn corner in Figure 5(i).

Graphene edges are of particular interest since their orientations determine the electronic properties. Crack extension with the formation of fresh edges is mainly caused by local high strain concentrated around crack-tips. Our simulations demonstrate that torn edges maintain straightness and cleanness along either zigzag or armchair direction and can change directions by 30° or multiples of 30°, in Figures 4 and 5, coincided with experiments.[14] Under pure opening loading ($\varphi = 90°$, in Figures 5(f) and 5(l)), the growth of zigzag crack is self-similar whereas armchair crack advances in an irregular manner, consistent with previous reports.[7] The direction of crack growth changes definitely under coupled opening and shearing stresses, and edges interconvert between ZZ and AC preferably along zigzag directions in agreement with previous simulations.[10,13] By Griffith criterion, this suggests lower edge energy in ZZ relative to AC, coincident with results by empirical potentials.[29,30,34] More abundant ZZ edges appeared is due to not only lower edge energy but also somewhat local residual stresses and dynamic fracture effects. Experiments also showed long-term stability[35] of ZZ edges, and more ZZ edges were initially formed at high temperatures.[36] Another experiment[37] also confirmed that the zigzag edge is more stable than the armchair edge, although the opposite has been predicted theoretically by *ab initio* calculations which depend strongly on the choice of the density functional among different DFT calculations yielding dramatically different values in quantitative scattering. In Ref. 14, the initial torn edges were along ZZ direction under pure mechanical stress during the graphene transfer process, while heating and chemical effects knock-on sputtering induced by electron irradiation in TEM inevitably influenced crack extension stimulated afterwards.

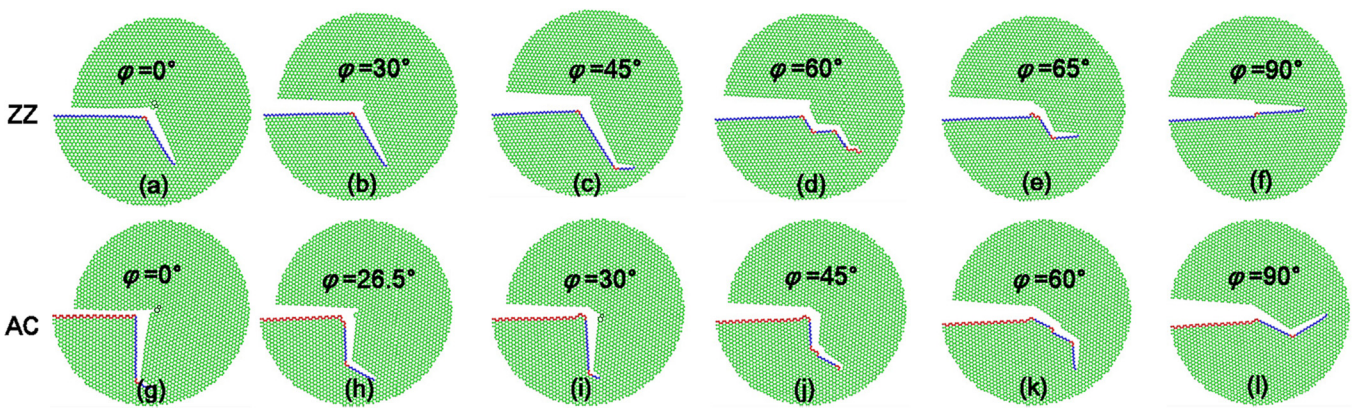

FIG. 5. Images of crack kinking in graphene lattices (green) after propagation in Figure 4 (after breakdown of the first bond in Figure 3, the crack-tip moves, the applied displacement loads are not precisely of the crack-tip asymptotic solution, stresses become more complex), ZZ (blue), or AC (red) edges appear alternatively changing direction of growth (enhanced online) [URL: http://dx.doi.org/10.1063/1.4754115.1] [URL: http://dx.doi.org/10.1063/1.4754115.2].

During our simulations, total energy at each strain level is minimized for each equilibrium lattice structure. The kinematic energy changes slightly while potential energy increases gradually since the temperature is coupled with a thermostat. Energy jumps are infrequently observed; thus, lattice-trapping effects are negligibly small for long-range potentials we used. Undoubtedly, temperature and strain rate can quantitatively affect K^c that increases slightly with increase of strain rates while decreases with temperature. At high temperature beyond 1000 K, fracture shows plastic behaviors opposite to brittle at room temperature, the crack edges are reconstructed, fresh surfaces are bridged with carbon chains, and formation and motion of defects and vacancies appear frequently.

In summary, graphene embedded with a pre-existing zigzag or armchair edge crack under complex mechanical stresses is studied by large amount MD simulations based on the modified REBO potential. An asymptotic expansion of the displacement field in the vicinity of crack tip is adopted to apply loading combined with in-plane opening and shear stresses. The critical effective stress intensity factors are obtained in the range of 2.63 nN $Å^{-3/2}$ to 3.38 nN $Å^{-3/2}$ varied with the phase angle of far-field loading, these predicted low toughness indicate that strong graphene is absolutely brittle at room temperature. The direction of crack initiation also depends on the phase angle and changes by 30° (or multiples of 30°) to the original crack line. Straight cracks with zigzag edges grow self-similarly when opening loading is dominant, or else kinking occurs. Torn edges of fresh cracks are along either zigzag or armchair orientations, while zigzag edges are more preferable. Fresh armchair edges are only formed occasionally under particular stress conditions. Therefore brittle fracture of graphene prefers along zigzag edges concerning with its lower toughness and applied complex mechanical stresses in dynamic rupture.

B.Z. gratefully acknowledges supports from Newton International Fellowship (NF080039) and Newton Alumni Follow-On of UK's Royal Society hosted by University of Glasgow and Newcastle University, and NSFs (10602023, 11172130, and 11232007), the Fundamental Research Funds for the Central Universities, the Program for Changjiang Scholars and Innovative Research Team (IRT0968) and National Basic Research Program (973, 2011CB707602) of China.

[1]K. S. Novoselov, A. K. Geim, S. V. Morozov, D. Jiang, Y. Zhang, S. V. Dubonos, I. V. Grigorieva, and A. A. Firsov, Science **306**, 666 (2004).
[2]Y. Pan, H. Zhang, D. Shi, J. Sun, S. Du, F. Liu, and H. Gao, Adv. Mater. **21**, 2777 (2009).
[3]C. Lee, X. Wei, J. W. Kysar, and J. Hone, Science **321**, 385 (2008).
[4]M. A. Rafiee, J. Rafiee, I. Srivastava, Z. Wang, H. Song, Z. Yu, and N. Koratkar, Small **6**, 179 (2010).
[5]A. Hashimoto, K. Suenaga, A. Gloter, K. Urita, and S. Iijima, Nature (London) **430**, 870 (2004).
[6]A. Omeltchenko, J. Yu, R. K. Kalia, and P. Vashishta, Phys. Rev. Lett. **78**, 2148 (1997).
[7]M. Xu, A. Tabarraei, J. T. Paci, J. Oswald, and T. Belytschko, Int. J. Fract. **173**, 163 (2012).
[8]S. Zhang, T. Zhu and T. Belytschko, Phys. Rev. B **76**, 94114 (2007).
[9]S. Huang, S. Zhang, T. Belytschko, S. S. Terdalkar, and T. Zhu, J. Mech. Phys. Solids **57**, 840 (2009).
[10]Q. Lu, W. Gao, and R. Huang, Modell. Simul. Mater. Sci. Eng. **19**, 54006 (2011).
[11]M. I. Katsnelson and A. K. Geim, Philos. Trans. R. Soc. London, Ser. A **366**, 195 (2008).
[12]G. Cocco, E. Cadelano, and L. Colombo, Phys. Rev. B **81**, 241412 (2010).
[13]D. Sen, K. S. Novoselov, P. M. Reis, and M. J. Buehler, Small **6**, 1108 (2010).
[14]K. Kim, V. I. Artyukhov, W. Regan, Y. Liu, M. F. Crommie, B. I. Yakobson, and A. Zettl, Nano Lett. **12**, 293 (2012).
[15]J. C. Meyer, F. Eder, S. Kurasch, V. Skakalova, J. Kotakoski, H. J. Park, S. Roth, A. Chuvilin, S. Eyhusen, G. Benner, A. V. Krasheninnikov, and U. Kaiser, Phys. Rev. Lett. **108**, 196102 (2012).
[16]D. W. Brenner, O. A. Shenderova, J. A. Harrison, S. J. Stuart, B. Ni, and S. B. Sinnott, J. Phys. Condens. Matter. **14**, 783 (2002).
[17]B. Zhang and W. Guo, Appl. Phys. Lett. **87**, 51907 (2005).
[18]W. Guo, C. Z. Zhu, T. X. Yu, C. H. Woo, B. Zhang, and Y. T. Dai, Phys. Rev. Lett. **93**, 245502 (2004).
[19]T. Chang and Z. Guo, Nano Lett. **10**, 3490 (2010).
[20]A. Shenderova, D. W. Brenner, A. Omeltchenko, X. Su, and L. H. Yang, Phys. Rev. B **61**, 3877 (2000).
[21]T. Belytschko, S. P. Xiao, G. C. Schatz, and R. Ruoff, Phys. Rev. B **65**, 235430 (2002).
[22]R. Grantab, V. B. Shenoy, and R. S. Ruoff, Science **330**, 946 (2010).
[23]H. Gao, B. Ji, I. L. J A Ger, E. Arzt, and P. Fratzl, Proc. Natl. Acad. Sci. U.S.A. **100**, 5597 (2003).
[24]M. L. Williams, J. Appl. Mech. **24**, 109 (1957).
[25]T. L. Anderson, *Fracture Mechanics: Fundamentals and Applications*, 2nd ed. (CRC, Boca Raton, FL, 1991), p. 54.
[26]L. Blakslee, D. G. Proctor, E. J. Seldin, G. B. Spence, and T. Weng, J. Appl. Phys. **41**, 3373 (1970).
[27]C. Liu and J. Nocedal, Math. Program. **45**, 503 (1989).
[28]A. Griffith, Philos. Trans. R. Soc. London, Ser. A **221**, 163 (1921).
[29]Q. Lu and R. Huang, Phys. Rev. B **81**, 155410 (2010).
[30]P. S. Branicio, M. H. Jhon, C. K. Gan, and D. J. Srolovitz, Modell. Simul. Mater. Sci. Eng. **19**, 54002 (2011).
[31]S. S. Terdalkar, S. Huang, H. Yuan, J. J. Rencis, T. Zhu, and S. Zhang, Chem. Phys. Lett. **494**, 218 (2010).
[32]J. Qian and A. Fatemi, Eng. Fract. Mech. **55**, 969 (1996).
[33]M. Engelund, J. A. F. U. Rst, A. P. Jauho, and M. Brandbyge, Phys. Rev. Lett. **104**, 036807 (2010).
[34]V. B. Shenoy, C. D. Reddy, A. Ramasubramaniam, and Y. W. Zhang, Phys. Rev. Lett. **101**, 245501 (2008).
[35]Ç. Ö. Girit, J. C. Meyer, R. Erni, M. D. Rossell, C. Kisielowski, L. Yang, C. H. Park, M. F. Crommie, M. L. Cohen, S. G. Louie *et al.*, Science **323**, 1705 (2009).
[36]X. Jia, M. Hofmann, V. Meunier, B. G. Sumpter, J. Campos-Delgado, J. M. Romo-Herrera, H. Son, Y. P. Hsieh, A. Reina, J. Kong *et al.*, Science **323**, 1701 (2009).
[37]Y. C. Cheng, H. T. Wang, Z. Y. Zhu, Y. H. Zhu, Y. Han, X. X. Zhang, and U. Schwingenschlögl, Phys. Rev. B **85**, 073406 (2012).